An analytical method for determining the tensile membrane action of RC slab panels

An analytical method for determining the tensile membrane action of RC slab panels

Yong Wang [a, b], Gongchen Wang [a], Zhaohui Huang [c, d*], Yuner Huang [e], Yaqiang Jiang [a], Yajun Zhang [a],
Cong Zhang [f], Yixiang Bu [a], Wei Song [a]

[a] *JiangSu Collaborative Innovation Center for Building Energy Saving and Construct Technology, Jiangsu, 221008, China*

[b] *State Key Laboratory for Geomechanics & Deep Underground Engineering, China University of Mining & Technology, Xuzhou, Jiangsu 221116, China*

[c] *Department of Civil and Environmental Engineering, Brunel University, Uxbridge, Middlesex, UB8 3PH, UK*

[d] *Vulcan Solutions Limited, Sheffield, S32 1DA, UK*

[e] *School of Engineering, The University of Edinburgh, Edinburgh, UK*

[f] *School of Environment and Civil Engineering, Jiangnan University, Jiangsu, 214122, China*

Abstract: This paper presents a newly developed method for determining the influence of tensile membrane action on the ultimate loading capacity of a two-way RC concrete slab. In this method, more realistic membrane action and two failure criteria of a slab panel are established. The developed method has been validated against the test results and good agreement is achieved. Compared to the tensile membrane action region obtained from the FEM (Vulcan), the assumptions about the focus of the ellipse equation proposed within the present method are reasonable and accurate. The present method can be used for predicting the ultimate loads and failure modes of the two-way simply supported RC slabs at large deflections. The research indicates that the in-plane shear force has considerable effect on the prediction of ultimate loads of the slabs and neglecting the in-plane shear force results the overestimated the concrete corner strains.

Keywords: two-way supported slabs; tensile membrane action; failure criterion; in-plane shear force; failure mode

* Corresponding author, Email address: zhaohui.huang@vulcan-solutions.com (Z. Huang)

Notation

a	Slab panel aspect ratio (L/l)
a_x	Height of concrete compression zone
A	Compression area
$A_{sx(y)}$	Reinforcement area per length in x (or y) direction
b	Membrane force parameter
C_1 , C_2	The concrete compressive force at yield line
d	Average effective depth of reinforcement (mm)
d_1 , d_2	Effective height of steel bar in both directions
e	Overall enhancement of theoretical yield-line load due to membrane action
e_1 , e_2	Enhancement coefficient
e_{1b} , e_{2b}	Bearing capacity coefficient of yield line
e_{1m} , e_{2m}	Increase coefficient of slab panel's load carrying capacity due to membrane force
E_c/E_s	Ratio of Young's modulus of concrete and reinforcement
EG (x_c)	Compressive membrane area
f_c	Cylinder compressive strength of concrete
f_{cu}	Cubic strength of concrete
f_y	Yield strength of steel reinforcement
g_0	Ratio of compressive stress area of concrete
g_1	Parameter defining the compressive stress block in flexural action (short span)
g_2	Parameter defining the compressive stress block in flexural action (long span)
h	Slab thickness
I_{cr}	Moment of inertia of cracked cross section
I_{eff}	Effective moment of inertia of cross section
k	Membrane force parameter
K	Ratio of yield force per unit width of reinforcement bar in y direction to yield force per unit width of reinforcement bar in x direction
$L(l)$	Longer (shorter) span of rectangular slab
M_{01} , M_{02}	Bending resistance moment without the effect of the membrane action
M_{1m}, M_{2m}	Moment resulted from vertical displacement

n	Factor defining the yield-line pattern
$N_{y'}$	Force at distance y
P	Uniformly distributed theoretical yield-line load
P_{limit}	Predicted ultimate load of slab panel
P_{limit}/P_{test}	The ratio between the calculated value of ultimate bearing capacity and the test value
P_{test}	Tested ultimate load of slab panel
S	Shear force
T_0	Yield force of reinforcement per unit width
T_1 , T_2	Resultant in-plane tension forces along the yield line
x, y, z	Coordinate axis of slab panel
Ø	Diameter of reinforcing bar
α	Angle defining the yield line pattern of slab panel
$\sigma_{c,max}$	Membrane force at point E
δ_{limit}	Predicted vertical mid-span displacement of slab panel
δ_{test}	Tested vertical mid-span displacement of slab panel
ε_1	Maximum compressive strain at the corners of slab panel (top surface)
ε_2	Compressive strain of concrete in the middle of slab panel
ε_{cu} or ε_{su}	Ultimate compressive concrete strain or steel strain
μ	Orthogonal parameter
φ	Major axis length
w	Deflection of the central region of slab panel
w_{total}	Total mid-span deflection of slab panel
w_{yield}	Mid-span displacement at initial yield (0.4 d_1)

1. Introduction

Tensile membrane action of reinforced concrete slabs subjected to large displacement has been investigated by many researchers [1-18]. For the tensile membrane action, there is no practical use under normal working conditions. However, under accidental loads, such as explosions and fire, the tensile membrane action can be mobilised, if designed correctly, allowing structural stability of buildings to be maintained. Thus, the topic has again acquired an important relevance as the reserve of bearing capacity that the tensile membrane action provides can become significant in the response of structures in extreme load conditions [4-18]. Unlike finite element models, the analytical methods can be easily applied in engineering design practice. So far, several analytical models were developed to consider the influence of tensile membrane action on the ultimate loading capacity of a two-way supported concrete slab panel. It is evident that each model has its own advantages and shortcomings, due to different assumptions and support conditions. For instance, Cameron and Usmani [10] assume that the slab panels have full boundary restraint. Li et. al. [11] propose that the edges of the slab panel are vertically supported, but horizontally restrained, such as the slab panel located in the interior of a building. However, for the slab panels located at the edge of the building, the simply supported boundary condition should be used to assess the loading capacities of the panels. Thus, to be conservative for design, several researchers [12-18] assume that the slab panels are simply supported at their four edges.

In terms of the failure mechanism of slab panels, several yield line failure patterns were proposed to determine the ultimate loading capacity of the slab panel, in which the

panel was divided into four [12], five [11, 13], six or eight [15-16] slab facets. Sawczuk and Winnicki [19] and Hayes [20] proposed two failure modes of a slab panel: 1) a large crack was formed across the shorter span of the slab panel at its center point; 2) two large cracks were formed across the shorter span of the panel at the two intersections of the yield lines. However, both models give over-predicted ultimate loading capacity of the slab panel [14-15]. Based on the test results of small-scale slab panels, Bailey and Toh [14] proposed a method which is a slightly modified version of Hayes' model. However, Bailey's method significantly underestimates the ultimate loading capacity of the slab panel [14, 21]. Omer et al. [15] assume the failure mode of the slab panel in which the additional full depth cracks are formed across the short span of the panel at different locations. In this model, the in-plane tensile forces are assumed to be distributed across the full width of the slab panel with the compressive forces being concentrated over a very small area near the edge of the slab panel. Clearly, this assumption does not agree with the experimental observations (concrete crushing near to the corners of slab panel) [1-4] and the results of numerical analyses [6-9].

In the model proposed by Li et al. [11], a slab panel is divided into five slab facets, including a slab facet with elliptic paraboloid shape. In this model, it is assumed that the yielding shape of bottom reinforcing steel is in elliptic shape. In fact, according to Ref. [22], at a limit state, the yielding shape of bottom reinforcing steel is in rectangular (square) shape. Wang et al. [13] proposed a model based on the steel strain difference approach. In the model a slab panel is also divided into five parts, including four rigid plates and a rectangular (square) region. The model assumes that the yield shape of

bottom reinforcing steel is in rectangular (or square) shape and the tensile membrane action region of slab panel is simply considered to be a rectangular (or square) shape. This assumption is not reasonable. Note that, different from the above methods (several rigid facets), Matteo et al. [26] proposed the slab strip model to assess the ultimate bearing capacity of reinforced concrete two-way slabs at large deflection, and two failure criteria were established, including the maximum ultimate slab strip elongation and the maximum ultimate rotation of the structure at the supports.

Based on the experimental observations [1-4], two failure criteria are often used to determine the ultimate loading capacity of a concrete slab panel, which are the tensile failure of reinforcing steel at center of the slab panel and the concrete crushing at the corners of the slab panel. A number of previously developed models [13-17, 21] adopted these two failure criteria with different interpretations and limitations. Recently, Burgess [18] proposed a method to determine the load-deflection curve (ascending and descending stages) of a lightly reinforced concrete slab panel. The method makes the conventional assumption of an unchanged yield-line mechanism (x-aligned or y-aligned mechanisms), and subsequently ensures equilibrium of the flat facets of the mechanism using the correct kinematics as the deflection increases. The fracture ductility of reinforcing mesh crossing yield lines is used to monitor the progressive fracture of the mesh across the yield-line cracks. This method was further developed to consider the effect of boundary restraint on the large-deflection behavior of lightly reinforced concrete slabs, and horizontal equilibrium of all of the flat facets of the slab is determined by the combination of forces across the yield lines within the slab and across

the slab edges [24, 25]. However, this method is assumed to apply to thin lightly reinforced slabs with a single layer of isotropic reinforcing mesh, and a steel area in either direction which is considerably less than 1% of the gross cross-section area, and thus the concrete compressive crushing at the corners cannot be predicted as well as the tensile or compressive membrane action region.

As discussed above, all these existing methods have different drawbacks, making them inaccurate and less suitable for practical purposes. For this reason, a new method for the assessment of a two-way simply supported slab panel is developed in this paper. Based on the experimental evidences and numerical results, in the current method, the tensile membrane action region is determined based on the proposed ellipse equations. Hence, the in-plane stress distribution can be reasonably estimated. In addition, two failure criteria are introduced to determine the failure modes of the slab panel which are related to concrete and steel. Also the effect of the in-plane shear force on the concrete compressive failure mode is also studied. Finally, the theoretical predictions are compared with the experimental results conducted by different researchers, and further verifications are conducted through the comparison with the numerical results.

2. Proposed method

2.1 Assumptions

The assumptions adopted in this method are summarized as follows:

(1) The slab is square or rectangular in plan, and the ratio between the length and width is not greater than three.

(2) The proposed failure mode in the rectangular concrete slab is shown as in Figs. 1(a)-

(b).

(3) For a rectangular slab panel, the central region of tensile membrane tractions is elliptical, as shown in Fig. 1(a). The intersecting points (Points *B* and *C*) of the yield line in the middle region are assumed to be the two foci of the elliptic equation, and (x_0, y_0) is the intersecting point of the yield line and the ellipse, as shown in Fig. 1(a).

(4) The force distribution of the slab at the ultimate limited state is shown in Figs. 2(a)-(c), and C_1 and C_2 are the concrete compressive forces between plates, respectively; T_1 and T_2 are the tensile forces of the steel bar, respectively; S is the in-plane shear force, and T_0 is the yield force of the steel.

Note that, the diagonal yield line can contain up to three distinct zones: a zone adjacent to the slab corner where only bending moments contribute internal work; a zone in which both moment and membrane force do work; a zone adjacent to the yield-line intersection where only tensile membrane force does work. The latter corresponds to the length of yield line in which there is no concrete stress block, which is particularly relevant at high deflections ($w \geqslant 0.6d$) [27].

(4) Two failure criteria, based on the deflection failure criterion and concrete crushing strain, are established to determine the ultimate loads and deflections of concrete slabs.

2.2 Ellipse equation

According to the yield line theory, the angle α in Fig. 2(a) is defined as:

$$\sin\alpha = nL / \left[\sqrt{(nL)^2 + \frac{l^2}{4}}\right], \quad n = \frac{1}{2\mu a^2}\left[\sqrt{1+3\mu a^2} - 1\right] \tag{1}$$

where n is the factor defining the yield-line pattern; L (l) is the length (width) of the slab; a is the aspect ratio of the slab (L/l) ; μ is the ratio of the yield moment capacity

of the slab in the orthogonal direction (M_{01}/M_{02}), and it is less than or equal to unity.

According to the numerical results [6-7], it is found that the distribution of membrane actions comprises tensile membrane traction in the central plan area of the slab surrounded by a balancing ring of compressive membrane stress. In the previous models, the in-plane force distribution along the yield line was often assumed by many researchers [14-18], and the in-plane shear force S was considered [13, 17, 24] or not [12].

Note that, in Bailey's model it was assumed that a full-depth crack along the short span of the slab panel occurs, and the compressive force C_2 (Fig. 2(c)) was acted at point E. However, the numerical analysis conducted by many researchers shows that a certain proportion across the short span of the slab is in compression, and this assumption may be not reasonable [14]. Hence, as shown in Fig. 2(c), a reasonable force distribution within the slab panel at the ultimate limit state is assumed. As shown in Fig. 1(a), the boundary between the regions of tensile and compressive membrane stress is defined by Points I_1、I_2、I_3 and I_4, and the coordinate of Point I_1 is (x_0, y_0). As shown in Figs. 2(a)-2(c), according to the in-plane (translational direction) force equilibrium (Eqs. 2(a)-2(b)), the following equations can be obtained as:

$$(T_1/2)\sin\alpha = C_1 - T_2 \quad \text{(direction: perpendicular to yield line CD)} \tag{2a}$$

$$(T_1/2)\cos\alpha = S \ \text{(direction: parallel to yield line CD)} \tag{2b}$$

$$T_1 = bKT_0(L-2nL) \tag{3a}$$

$$C_1 = \frac{kbKT_0}{2}\left(\frac{k}{1+k}\right)\sqrt{(nL)^2+\frac{l^2}{4}} \tag{3b}$$

$$T_2 = \frac{bKT_0}{2}\left(\frac{1}{1+k}\right)\sqrt{(nL)^2 + \frac{l^2}{4}} \tag{3c}$$

$$k = \frac{4na^2(1-2n)}{4n^2a^2+1} + 1 \tag{3d}$$

where k is the parameter defining magnitude of membrane force, which can be obtained from the in-plane force equilibrium of Plate ① (direction: perpendicular to yield line BC); T_0 is the yield force in reinforcing steel per unit width (kN/m) in the long span direction; C_1 is the concrete compressive force at the yield line; T_1 (T_2) is the resultant in-plane tension forces along the yield line BC (BI_1); b is the parameter defining magnitude of membrane force; n is the parameter defining the yield line; L is the longer span of rectangular slab; l is the shorter span of rectangular slab; K is the ratio of yield force in the reinforcing steel of the short span to the yield force in the reinforcing steel of the long span; a is the aspect ratio (L/l); $\boldsymbol{\alpha}$ is the angle defining the yield line pattern; S is the in-plane shear force along a diagonal yield line.

According to the geometric equation, the coordinates of Point I_1 (x_0, y_0) can be calculated as:

$$x_0 = L_{AE} - L_{AQ} = \frac{L}{2} - \frac{knL}{1+k}, \quad y_0 = L_{BJ} = \frac{l}{2(1+k)} \tag{4}$$

As indicated in Fig. 1(a), the shape of the region of tensile membrane traction at the ultimate limited state is elliptic. Therefore, four points I_1 to I_4 can be used to establish the elliptic equation. Clearly, based on this four points, the elliptic equation cannot be determined, and another key point should be chosen. Thus, based on the general yield-line theory, two intersection points (Points B and C) are assumed to be two foci of the elliptic equation. Hence, the elliptic equation can be determined as:

$$\frac{x^2}{L_{FR}^{\ 2}}+\frac{y^2}{L_{FG}^{\ 2}}=1 \quad , \quad L_{FG}\leq l/2,\ L_{FR}\leq L/2 \tag{5}$$

Using two foci (Points B and C) and Point I_1 (x_0, y_0), Equation (5) can be represented as:

$$\sqrt{\left(x_0-\left(\frac{L}{2}-nL\right)\right)^2+y_0^{\ 2}}+\sqrt{\left(x_0+\left(\frac{L}{2}-nL\right)\right)^2+y_0^{\ 2}}=2\varphi \tag{6a}$$

$$\varphi^2-\left(\frac{L}{2}-nL\right)^2\leq\frac{l^2}{4} \tag{6b}$$

where φ is the length of the major axis.

In this method, the width of the compressive membrane force at slab edges (L_{EG}) is defined as x_c ($\geq$0), as shown in Fig. 2(c).

2.3 Force equilibrium

As shown in Fig. 2(c), for Plate ③, the distribution of compressive membrane stress is triangular, and its maximum value at the edge (Point E) is assumed to be $\sigma_{c,max}$, and thus the equilibrium equation (x direction) is defined as:

$$C_2=\frac{\sigma_{c,max}x_c}{2}=KT_0\left(\frac{l}{2}-x_c\right)+C_1\cos\alpha-T_2\cos\alpha-S\sin\alpha \tag{7}$$

Or

$$C_2=\frac{\sigma_{c,max}x_c}{2}=\frac{KT_0}{4}[2l-4x_c+\frac{k^2bl}{1+k}-\frac{bl}{1+k}-\frac{nblL^2\left(1-2n\right)}{\left(nL\right)^2+(l/2)^2}] \tag{8}$$

where C_2 is the resultant in-plane compression force; $\sigma_{c,max}$ is the maximum compressive membrane stress at the edge of the slab or Point E; x_c is the width (L_{EG}) of the compressive membrane stress. Note that, according to the numerical results, the triangular distribution of compressive traction towards the slab edge is assumed in this paper, as discussed later.

As shown in Fig. 2(c), for Plate ③, taking moments about E, and it is:

$$T_2\left[\left(\frac{\cos\alpha\times L}{2}-\frac{\frac{L}{2}-nL}{\cos\alpha}\right)\frac{1}{\tan\alpha}-\frac{\sqrt{(nL)^2+\frac{l^2}{4}}}{3(1+k)}\right]-KT_0\left(\frac{1}{2}-x_c\right)\left(\frac{1}{4}+\frac{x_c}{2}\right)$$
$$+\frac{1}{3}C_2x_c-\frac{T_1}{4}\left(\frac{L}{2}-nL\right)+C_1\left[\frac{\sin\alpha L}{2}-\frac{k\sqrt{(nL)^2+\frac{l^2}{4}}}{3(l+k)}\right]+S\frac{L}{2}\cos\alpha=0 \quad (9)$$

Substituting for T_1 (Eq. 3(a)), T_2 (Eq. 3(c)), C_1 (Eq. 3(b)), C_2 (Eq. 7) and S (Eq. 2(b)) into Eq. (9), b can be obtained as:

$$b=\frac{\left(\frac{l}{2}-x_c\right)\left(\frac{l}{4}+\frac{x_c}{2}\right)-\frac{x_c(l-2x_c)}{6}}{A-B+C+D+E} \quad (10)$$

where

$$A=\frac{x_c\left(k^2l-l\right)}{12(1+k)}-\frac{x_cnlL^2(1-2n)}{12\left((nL)^2+(l/2)^2\right)},\quad B=\frac{1}{2}\left(\frac{L}{2}-nL\right)^2$$

$$C=\frac{1}{2(1+k)}\left[\frac{l^2}{8n}-\frac{L-2nL}{2nL}\left((nL)^2+(l/2)^2\right)-\frac{(nL)^2+(l/2)^2}{3(1+k)}\right]$$

$$D=\frac{k^2}{2(1+k)}\left[\frac{nL^2}{2}-\frac{k\left((nL)^2+(l/2)^2\right)}{3(1+k)}\right],\quad E=\frac{l^2L^2(1-2n)}{16\left[(nL)^2+(l/2)^2\right]}$$

As shown in Figs. 3(a)-(b), the moment without the effect of the membrane action (M_{01} and M_{02}) are defined as:

$$M_{01}=KT_0d_1\left(\frac{3+g_1}{4}\right),\quad M_{02}=T_0d_2\left(\frac{3+g_2}{4}\right) \quad (11a)$$

$$g_1=\left[\frac{d_1}{2}-\frac{KT_0}{f_{cu}}\right]\Big/\frac{d_1}{2}\quad g_2=\left[\frac{d_2}{2}-\frac{T_0}{f_{cu}}\right]\Big/\frac{d_2}{2} \quad (11b)$$

,

where M_{01} and M_{02} are the moment of resistance (no axial force) in the short and long spans, respectively, as shown in Appendix A; d_1 and d_2 are the effective depth of reinforcement in the short and long spans, respectively; f_{cu} is the compressive cube strength of concrete; g_1 and g_2 are parameters defining the compressive stress block in flexural action in the short and long spans, respectively.

As shown in Figs. 4(a)-(b) and Appendix A, for a given maximum vertical displacement

w, the moments (M_{1m} and M_{2m}) about the supports due to the membrane forces are given by:

$$M_{1m}=KT_0Lbw[(1-2n)+\frac{n(3k+2)}{3(1+k)^2}-\frac{nk^3}{3(1+k)^2}-\frac{l^2(1-2n)}{8\left[(nL)^2+(l/2)^2\right]}] \tag{12}$$

$$M_{2m}=KT_0lbw[\frac{2+3k}{6(1+k)^2}-\frac{k^3}{6(1+k)^2}+\frac{nL^2(1-2n)}{4\left[(nL)^2+(l/2)^2\right]}] \tag{13}$$

The above expressions (Eqs. (12) and (13)) are divided by $M_{01}L$ and $M_{02}l$, respectively, the enhancement factors e_{1m} (Plate ①) and e_{2m} (Plate ②) are defined as:

$$e_{1m}=\frac{M_{1m}}{M_{01}L}=\frac{4b}{3+g_1}\left(\frac{w}{d_1}\right)[1-2n+\frac{n(2-k)}{3}-\frac{l^2(1-2n)}{8[(nL)^2+(l/2)^2]}] \tag{14}$$

$$e_{2m}=\frac{M_{2m}}{M_{02}l}=\frac{2Kb}{3+g_2}\left(\frac{w}{d_2}\right)[\frac{2-k}{3}+\frac{nL^2(1-2n)}{2[(nL)^2+(l/2)^2]}] \tag{15}$$

where e_{1m} and e_{2m} are the enhancement factors of Plates ① and ② due to membrane action, respectively.

For Plates ① and ②, if the axial compressive force N is present, the moment capacity is given by:

$$\frac{M}{M_0}=1+\alpha'(\frac{N}{T_0})-\beta'(\frac{N}{T_0})^2 \tag{16a}$$

$$\alpha'=\frac{2\times g_0}{3+g_0},\quad \beta'=\frac{1-g_0}{3+g_0} \tag{16b}$$

where g_0 is the parameter fixing depth of compressive stress block when no membrane force is present.

As shown in Fig. 5(a), for Plate ①, for the yield line AB, the distance between B and the projection (x axis) is x', and the membrane force $N_{x'}$ is:

$$N_{x'}=bKT_0(\frac{x'(k+1)}{nL}-1) \tag{17}$$

Thus, the moment contribution for AB and CD (Fig. 2(a)) is:

$$Z=2\int_0^{nL}\frac{M}{M_0}dx'=2nL\left[1+\frac{\alpha'_1 b}{2}(k-1)-\frac{\beta'_1 b^2}{3}(k^2-k+1)\right] \tag{18a}$$

$$\alpha'_1=\frac{2\times g_1}{3+g_1},\quad \beta'_1=\frac{1-g_1}{3+g_1} \tag{18b}$$

where Z is the contribution due to the enhanced bending capacity, in the areas where in-plane compressive stress occurs; M_0 is the moment of resistance when no axial force is present. If M is divided by M_0L, an enhancement factor due to the effect of the membrane forces is obtained. Note that, the effect of membrane forces on the bending resistance will be considered separately for each yield line.

Similarly, for the yield line BC in Fig. 2(a), the membrane force is constant, N=-bKT_0, and we have

$$Y=\frac{M}{M_0}=(L-2nL)(1-\alpha'_1 b-\beta'_1 b^2) \tag{19}$$

For the yield line GF in Fig. 2(c), the membrane force is constant, N=-KT_0, and we have

$$\frac{M}{M_0}=1-K\alpha'_2-\beta'_2 K^2 \tag{20a}$$

$$\alpha'_2=\frac{2\times g_2}{3+g_2},\quad \beta'_2=\frac{1-g_2}{3+g_2} \tag{20b}$$

Thus, according to three terms, i.e., Eqs. (18), (19) and (20), the enhancement factor e_{1b} is defined as:

$$e_{1b}=\frac{M}{M_0L}=\frac{Z}{L}+\frac{Y}{L}+\frac{2}{l}(1-K\alpha'_2-K^2\beta'_2)(\frac{l}{2}-x_c) \tag{21}$$

For Plate ②, across the yield line AB in Fig. 5(b), at a distance of y' from A, the membrane force $N_{y'}$ is:

$$N_{y'}=bKT_0(\frac{2y'(k+1)}{l}-1) \tag{22}$$

Similarly, for Plate ②, the moment contribution for $A'B$ and AB is:

$$2\int_0^{l/2}\frac{M}{M_0}\mathrm{d}y'=l\left[1+\frac{\alpha'_2 bK}{2}(k-1)-\frac{\beta'_2 b^2K^2}{3}(k^2-k+1)\right] \tag{23}$$

Thus, the enhancement factor e_{2b} is:

$$e_{2b}=\frac{M}{M_0 l}=1+\frac{\alpha'_2 bK}{2}(k-1)-\frac{\beta'_2 b^2K^2}{3}\left(k^2-k-1\right) \tag{24}$$

In all, the increases in strength in unrestrained slab arise partly from the tensile membrane action produced in the central region of the slab and partly from the increased yield moment in the outer regions where compressive membrane action is caused. On one hand, by taking the moments about the slab edges, the load capacities of each of the plates, due only to the membrane forces and their lever arms about the edges, are established, i.e., e_{1m} and e_{2m}. On the other hand, the load capacities of the plates due to the plastic bending moments distributed along the yield lines, amended by the presence of the coincident membrane forces, are not included in e_{1m} and e_{2m} but are aggregated as separate two factors, i.e., e_{1b} and e_{2b}.

2.4 Ultimate loads

According to the yield line theory, the ultimate load P of the slab is defined as:

$$P=\frac{24\mu M_0}{l^2}\left[\sqrt{3+\frac{1}{\mu a^2}}-\frac{1}{\sqrt{\mu}a}\right]^{-2} \tag{25}$$

As indicated in Eqs. (14), (15), (21) and (24), the dimension (non-dimensional form) of four enhancement factors (e_{1b}, e_{2b}, e_{1m} and e_{2m}) was the same. In addition, four enhancement factors were essentially related to the bending moment or moment equilibrium [27], including the moment about the support and the moment considering the effect of in-plane forces. Thus, considering the contribution of both membrane and bending effects, the enhancement factors for Plates ① and ② are given by:

$$e_1=e_{1m}+e_{1b}\ ,\ e_2=e_{2m}+e_{2b} \tag{26}$$

where e_1 and e_2 represent the enhancement resulted from tensile membrane action on the load capacity for the trapezoidal and the triangular plates, respectively. Note that,

considering the shear force interaction between the plates, Hay [20] proposed one enhancement factor e (e_1-(e_1-e_2)/(1+2μa^2)), but the derivation of the equation was not given.

Here, according to the force equivalence principle, the simply enhancement factor equation is proposed as:

$$P\left(2e_1A_1+2e_2A_2\right)=P_{\text{limit}}\left(L\times l\right) \tag{27}$$

where A_1 and A_2 are the areas of Plates ① and ②, respectively.

Thus, we have

$$P_{\text{limit}}=e\times P \tag{28}$$

$$e=(1-n)e_1+ne_2 \tag{29}$$

2.5 Failure criteria

As discussed in Refs. [13-14], two kinds of failure modes were observed in the small-scale slab tests, including the fracture of reinforcement at the centre of the slab and the compressive failure of concrete at the corners of the slabs. In some cases, the concrete crushing failure occurred at the area around E position (Fig. 2 (c)) subjected to pure axial compressive forces. Note that, such failures occur in heavily reinforced slabs [17]. Thus, this paper considers the following failure modes to determine the ultimate loading capacities of the concrete slabs.

(1) Compressive failure due to concrete crushing

Compressive failure along the compression ring is assumed at the slab corners and area around E position, and two concrete strains ($\boldsymbol{\varepsilon}_{\text{corner}}$ and $\boldsymbol{\varepsilon}_{\text{edge}}$) are proposed at the limit states, as shown in Fig. 2(c). Failure is identified if $\boldsymbol{\varepsilon}_{\text{corner}}$ or $\boldsymbol{\varepsilon}_{\text{edge}}$ > ε_{cu} (maximum

concrete compressive strain).

As shown in Appendix A, ε_{corner} is estimated assuming elastic behaviour of the concrete under the combined action of bending moments and axial forces, and it is defined as:

$$\varepsilon_{corner} = k_{corner}[\frac{C_1}{AE_c} + a_{x1}\frac{M_C}{E_c I_{eff}}] = k_{corner}[\frac{f_c}{E_c} + a_{x1}\frac{C_1 \times [h_0 - (a_{x1}/2)]}{E_c I_{eff}}], \quad E_c = \frac{10^{11}}{2.2 + \frac{34.74}{f_{cu}}} \tag{30a}$$

$$I_{eff} = \frac{I_{cr}}{2} \times (1.0 + \frac{w_{yield}}{w_{total}}), \quad I_{cr} = \frac{[(L/2 - x_0)/\sin\alpha]a_{x1}^3}{3} + \frac{E_s}{E_c}A_s(h_0 - a_{x1})^2 \tag{30b}$$

$$a_{x1} = \frac{C_1}{\alpha_1 f_c L_{AB}}$$

where k_{corner} is one modification factor (= 4.0); I_{eff} is the effective moment of inertia of the cross section; I_{cr} is the moment of inertia of the cracked cross section; E_c is the Young's modulus of concrete; E_s is the Young's modulus of steel; f_{cu} is the cubic strength of concrete; w_{yield} is the deflection corresponding to the yield load; w_{total} is assumed to be $l/20$; a_x is the depth of the compression zone.

As shown in Appendix A, ε_{edge} is defined as:

$$\varepsilon_{edge} = k_{edge}[\frac{C_2}{AE_c} + a_{x2}\frac{M_C}{E_c I_{eff}}] = k_{edge}[\frac{f_c}{E_c} + a_{x2}\frac{C_2(d_1 - a_{x2}/2)}{E_c I_{eff}}] \tag{31}$$

$$a_{x2} = \frac{C_2}{\alpha_1 f_c L_{EG}}$$

where k_{edge} is one modification factor (2.0).

As discussed in Ref. [13], the ultimate compressive strain ε_{cu} ranged from 0.0033 to 0.0038. Thus, one predefined value (such as 0.0035 or 0.0038) was often used to judge the compressive failure mode of the concrete slabs. However, this method is relatively random, since the concrete with different compressive strengths has different ultimate strains. Thus, according to Ref. [23], the concrete compressive ultimate strain $\boldsymbol{\varepsilon}_{cu}$ is defined as:

$$\frac{\varepsilon_{cu}}{\varepsilon_{c,r}} = \frac{1}{2\alpha_c}(1+2\alpha_c+\sqrt{1+4\alpha_c}) \quad (32a)$$

$$\varepsilon_{c,r} = (700+172\sqrt{f_c})\times 10^{-6}, \quad \alpha_c = 0.157 f_c^{0.785} - 0.905 \quad (32b)$$

where ε_{cu} is the ultimate compressive strain; $\boldsymbol{\varepsilon}_{c,r}$ is the peak strain of the concrete; $\boldsymbol{\alpha}_c$ is the parameter; f_c is the compressive cylinder strength of concrete.

(2) Reinforcement failure

To define the steel failure mode of slab, the ultimate steel strain ε_{su} at mid-span must be considered, such as 0.01 [23]. In fact, to define the reinforcing steel failure mode, the limiting mid-span deflection of the slab (l/20) is used in this paper [13]. In other words, the original length of the reinforcement (shorter span) is l, and the curved length l_c is l [1+($8w^2/3l^2$)] and its strain ($\boldsymbol{\varepsilon}_s$) is $8w^2/3l^2$. According to Ref. [23], $\boldsymbol{\varepsilon}_s$ approaches the ultimate strain 0.01, it is assumed that the fracture of the reinforcement occurs in the central region of the slab, and the corresponding mid-span deflection is about l/20.

In all, the maximum mid-span deflection (w) of the slab is assumed to be l/20, if the concrete compressive strain at the corners is larger than ε_{cu}, then the concrete crushing occurs, otherwise it is considered to be the reinforcement failure mode. In addition, the flow chart for predicting the ultimate loads and vertical displacements of concrete slabs is shown in Fig. 6.

3. Validation and discussion

Results from full-scale and small-scale concrete slab tests conducted by different authors are used for this validation. In addition, the finite element software (Vulcan [6-7]) was used to model the concrete slabs. The details of the nonlinear FE model can be found in the Refs [6-7].

3.1 Comparison of proposed method with experimental and theoretical results

As shown in Table 1, 32 concrete slabs [1, 2, 4, 5] are used in this paper because they are widely accepted to validate new methods. Fig. 7 presents the ultimate loads of several concrete slabs predicted by the current method together with the results generated by different methods. As shown in Table 2, the predictions of P_{limit} and δ_{limit} by different theories are compared against the experimental results (P_{test} and δ_{test}). The results are summarized as follows:

(1) As shown in Table 2, all the slabs sustained a load above the yield line, and the ultimate loads obtained from Bailey's method are significantly underestimated. For the present method (Present) in which the in-plane shear force is considered the predicted limit loads are basically agreed well with the experimental values, and the corresponding ratio (P_{limit}/P_{test}) ranged from 0.59 to 1.58, with the average value (Coefficient of Variation) of 0.98 (0.21). This comparison indicates that the predictions of proposed method is reasonable. On the other hand, as the in-plane shear force is not considered (Present *), the predicted loads are slightly lower, with the average value (Coefficient of Variation) of 0.92 (0.29).

(2) As shown in Fig. 7, the ultimate displacements obtained from Bailey's method are significantly underestimated. For instance, for the M-series (S-series) slabs, the ultimate displacements at the maximum loads ranged from 19.6 (46.5) to 85.4 (186.5) mm, with the average value of 52.1 (116.7) mm. In fact, for most of the slabs, their ultimate displacements were larger than 55 mm. However, the ultimate displacements of M-series (S-series) slabs predicted by Bailey methods ranged from 21.2 (17.1) to 44

(41.1) mm, with the average value of 28.9 mm (about span/40). In fact, the maximum mid-span deflection of most tested slabs at failure was often larger than span/20 [1-4], since the membrane action of the two-way slabs sufficiently developed at larger deflection.

3.2 Comparison with numerical results

Figs. 7(a)-7(h) show the comparison between the test results, the present method, Bailey's method and the numerical results. In the figure, the 'Proposed method' represents the in-plane shear force is considered and the 'Proposed method*' represents the in-plane shear force is ignored. Clearly, the numerical method reasonably predicted the load-displacement response of each slab. Bailey's method leads to conservative predictions due to the unreasonable failure mode and failure criteria adopted. As discussed above, for Bailey's method, the in-plane forces are tensile across the full width of the slab with the compressive force being concentrated over a very small area near the edge of the slab, as shown in Figs. 8(a) and 8(b). However, the numerical results show that a greater proportion at the supported edges of slab panel is in compression, as shown in Figs. 9(a)-9(i). In addition, it can be seen that the compressive membrane traction towards the slab edge gradually increases, and thus the triangular distribution of compressive traction (C_2) is assumed, as indicated in Fig. 2(c).

As discussed above, for the proposed method, x_0 and y_0 are two key parameters in determining the tensile membrane action region of concrete slabs. Therefore, the results from the numerical model were used to verify the rationality of these two parameters as predicted by the proposed method. The blue (red) arrow indicates the compressive

(tensile) membrane tractions of the concrete slab. In these plots, the lengths of the vectors are proportional to their magnitudes.

In addition, x_0 (or y_0) and the corresponding area predicted by the proposed method and numerical model are shown in Table 3. The value of A_1/A_2 ranges from 0.71 to 1.48, with an average ratio (Coefficient of Variation) of 0.94 (0.15), indicating that the values of x_0 and y_0 for the concrete slabs obtained using the proposed method are basically agreed well with those predicted by Vulcan.

3.3 Failure modes

The failure modes predicted by different methods are shown in Table 4 in which R represents the tensile failure of reinforcing steel and C represents the compressive failure of concrete. Clearly, Bailey's method cannot predict failure mode accurately. For instance, for Bailey's method, Slabs S3 to S10 were governed by reinforcement failure. In fact, only concrete crushing modes were observed from the *S*-series slabs due to the higher reinforcement ductility and reinforcement ratio. In contrast, the estimated failure modes of the proposed models are agreed well with experimental results for the most of the slabs. In addition, the effect of the in-plane shear force on the failure mode was studied, as shown in Table 4 and Figs. 7(a)-7(h), it is evident that it has a little influence on the failure mode.

Apart from $\boldsymbol{\varepsilon}_{\text{corner}}$, the present method can reasonably predict the strain $\boldsymbol{\varepsilon}_{\text{edge}}$, and $\boldsymbol{\varepsilon}_{\text{edge}}$ of all slabs were smaller than $\boldsymbol{\varepsilon}_{\text{corner}}$, and the crushing failure at Point *E* did not appear. In general, this conclusion is consistent with the experimental observation, no crushing failure appeared at the middle region of the edge, as shown in Figs. 10(a) and 10(b). In

all, compared to the concrete strength failure criterion [14, 16], using concrete compressive strain is more reasonable and effective, since the concrete crushing is governed by the ultimate compressive strain.

4. Conclusions

Based on the results of this study, the following conclusions can be drawn:

(1) The new analytical method, based on the proposed ellipse equation and failure criteria, is capable to predict the ultimate loads and deflection of the two-way supported concrete slabs.

(2) The developed method can be used for predicting the ultimate loads and failure modes of the two-way simply supported RC slabs at large deflections.

(3) The method can reasonably predict the tensile membrane action region and failure modes of the two-way concrete slabs. The prediction is agreed well with the numerical results.

(4) The in-plane shear force has little effect on the failure mode of concrete slabs. However, neglecting the shear force leads to higher ultimate loads and larger concrete corner strains.

Acknowledgements

This research was supported by the National Natural Science Foundation of China (Grant No. 51408594). The authors gratefully appreciate these supports.

Appendix A

***M_{01} and M_{02}* are equal to:**

$$C = \alpha_1 f_c b x$$

$$KT_0 = f_{cu}\left(\frac{d_1}{2} - \frac{d_1}{2} g_1\right)$$

$$g_1 = \frac{\frac{d_1}{2} - \frac{KT_0}{f_{cu}}}{\frac{d_1}{2}}$$

$$M_{01} = KT_0\left(d_1 - \frac{\frac{d_1}{2} - \frac{d_1}{2} g_1}{2}\right) = \frac{KT_0 d_1 (3 + g_1)}{4}$$

$$T_0 = f_{cu}\left(\frac{d_2}{2} - \frac{d_2}{2} g_2\right)$$

$$g_2 = \frac{\frac{d_2}{2} - \frac{T_0}{f_{cu}}}{\frac{d_2}{2}}$$

$$M_{02} = KT_0\left(d_2 - \frac{\frac{d_2}{2} - \frac{d_2}{2} g_2}{2}\right) = \frac{T_0 d_2 (3 + g_2)}{4}$$

where M_{01} (M_{02}) is the moment of resistance when no membrane force is present; KT_0 is the force in steel per unit width; g_1 (g_2) is the parameter defining the compressive stress block in flexural action in the short (long) span; d_1 (d_2) is the effective depth of reinforcement in the short (long) span; f_{cu} is the compressive cube strength of concrete; K is the ratio of yield force in the reinforcing steel in the short span to the yield force in the reinforcing steel in the long span.

M_{1m} is equal to:

$$M_{1m}=2T_2\sin\alpha\,h_2+T_1 w-2C_1\sin\alpha\,h_1-2S\cos\alpha\frac{w}{2}=2\times\frac{bKT_0}{2}\times\frac{1}{1+k}\times\sqrt{(nL)^2+(l/2)^2}\times\frac{nL}{\sqrt{(nL)^2+(l/2)^2}}$$
$$\times\frac{\frac{l}{2}-\frac{1}{3}\times\frac{1}{1+k}\times\sqrt{(nL)^2+(l/2)^2}\times\frac{l/2}{\sqrt{(nL)^2+(l/2)^2}}}{l/2}\times w+bKT_0(L-2nL)w-2\times\frac{kbKT_0}{2}\times\frac{k}{1+k}\times\sqrt{(nL)^2+(l/2)^2}$$
$$\times\frac{nL}{\sqrt{(nL)^2+(l/2)^2}}\times\frac{\frac{1}{3}\times\frac{k}{1+k}\times\sqrt{(nL)^2+(l/2)^2}\times\frac{l/2}{\sqrt{(nL)^2+(l/2)^2}}}{l/2}\times w-2\times\frac{bKT_0}{2}\times(L-2nL)\times\frac{l/2}{\sqrt{(nL)^2+(l/2)^2}}\times\frac{l/2}{\sqrt{(nL)^2+(l/2)^2}}\times\frac{w}{2}$$
$$=2\times\frac{bKT_0Lw}{2}\times\frac{n}{1+k}\times\left(1-\frac{1}{3(1+k)}\right)+bKT_0Lw(1-2n)-2\times\frac{bKT_0Lw}{2}\times\frac{nk^2}{1+k}\times\frac{k}{3(1+k)}-2\times\frac{bKT_0Lw}{2}\times(1-2n)\times\frac{l/8}{(nL)^2+(l/2)^2}$$
$$=bKT_0Lw\left[\frac{n}{1+k}\times\frac{3(1+k)-1}{3(1+k)}+(1-2n)-\frac{nk^3}{3(1+k)^2}-\frac{l^2(1-2n)}{8\left[(nL)^2+(l/2)^2\right]}\right]$$
$$=bKT_0Lw\left[\frac{n(2+3k)}{3(1+k)^2}+1-2n-\frac{nk^3}{3(1+k)^2}-\frac{l^2(1-2n)}{8\left[(nL)^2+(l/2)^2\right]}\right]$$
$$=bKT_0Lw\left[\frac{n(3-k)}{3}+1-2n-\frac{l^2(1-2n)}{8\left[(nL)^2+(l/2)^2\right]}\right]$$

where M_{1m} is the moment about support due to membrane forces for Plate ①; L (l) is the longer (shorter) span of the rectangular slab; w is the central vertical deflection; h_1 (h_2) is the lever arm about the edge (Figs. 4(a) and 4(b)).

M_{2m} is equal to:

$$M_{2m}=2T_2\cos\alpha\,h_2-C_1\cos\alpha\,h_1+S\sin\alpha\frac{w}{2}=2\times\frac{bKT_0}{2}\times\frac{1}{1+k}\times\sqrt{(nL)^2+(l/2)^2}\times\frac{\frac{l}{2}}{\sqrt{(nL)^2+(l/2)^2}}$$
$$\times\frac{nL-\frac{1}{3}\times\frac{1}{1+k}\times\sqrt{(nL)^2+(l/2)^2}\times\frac{nL}{\sqrt{(nL)^2+(l/2)^2}}}{nL}\times w-2\times\frac{kbKT_0}{2}\times\frac{k}{1+k}\times\sqrt{(nL)^2+(l/2)^2}$$
$$\times\frac{l/2}{\sqrt{(nL)^2+(l/2)^2}}\times\frac{\frac{1}{3}\times\frac{k}{1+k}\times\sqrt{(nL)^2+(l/2)^2}\times\frac{nL}{\sqrt{(nL)^2+(l/2)^2}}}{nL}\times w+2\times\frac{bKT_0}{2}\times(L-2nL)\times\frac{l/2}{\sqrt{(nL)^2+(l/2)^2}}\times\frac{nL}{\sqrt{(nL)^2+(l/2)^2}}\times\frac{w}{2}$$
$$=2\times\frac{bKT_0Lw}{2}\times\frac{1}{2(1+k)}\times\left(1-\frac{1}{3(1+k)}\right)-2\times\frac{bKT_0Lw}{2}\times\frac{k^2}{1+k}\times\frac{k}{6(1+k)}+2\times\frac{bKT_0Lw}{2}\times(1-2n)\times\frac{nL^2/4}{(nL)^2+(l/2)^2}$$
$$=bKT_0Lw\left[\frac{3k+2}{6(1+k)^2}-\frac{k^3}{6(1+k)^2}+\frac{nL^2(1-2n)}{4\left[(nL)^2+(l/2)^2\right]}\right]$$

where M_{2m} is the moment about support due to membrane forces for Plate ②.

ε_{corner} is equal to:

$$a_{x1}=\frac{C_1}{f_c\left(L/2-x_0\right)/\sin\alpha}$$

$$I_{cr}=\frac{L_{AB}a_{x1}^3}{3}+\alpha_{ES}A_S\left(d_1-a_{x1}\right)^2=\frac{\left[\left(L/2-x_0\right)/\sin\alpha\right]a_{x1}^3}{3}+\frac{E_S}{E_C}A_S\left(d_1-a_{x1}\right)^2$$

$$M_C=C_1\left(d_1-a_{x1}/2\right)$$

$$I_{eff}=\frac{I_{cr}}{2}\times(1.0+\frac{w_{yield}}{w_{total}})$$

$$\varepsilon_{corner}=k_{corner}[\frac{C_1}{AE_c}+a_{x1}\frac{M_C}{E_cI_{eff}}]=k_{corner}[\frac{f_c}{E_c}+a_{x1}\frac{C_1\times[h_0-(a_x/2)]}{E_cI_{eff}}]$$

where $\boldsymbol{\varepsilon}_{corner}$ is the maximum compressive strain at the corners of the slab; I_{eff} is the effective moment of inertia of the cross section; $I_{cr,x}$ is the moment of inertia of the cracked cross-section (x-direction) during the cracking stage; k_{corner} is the modification factor (4.0); w_{total} is the total mid-span deflection of the slab; w_{yield} is the mid-span deflection corresponding to the initial yield load.

$\boldsymbol{\varepsilon}_{edge}$ is equal to:

$$a_{x2}=\frac{C_2}{f_cx_c}$$

$$I_{cr}=\frac{x_ca_{x2}^3}{3}+\alpha_{ES}A_S\left(d_1-a_{x2}\right)^2=\frac{\left[\left(L/2-x_0\right)/\sin\alpha\right]a_{x2}^3}{3}+\frac{E_S}{E_C}A_S\left(d_1-a_{x2}\right)^2$$

$$M_C=C_2\left(d_1-a_{x2}/2\right)$$

$$I_{eff}=\frac{I_{cr}}{2}\times(1.0+\frac{w_{yield}}{w_{total}})$$

$$\varepsilon_{edge}=k_{edge}[\frac{C_2}{AE_c}+a_{x2}\frac{M_C}{E_cI_{eff}}]=k_{edge}[\frac{f_c}{E_c}+a_{x2}\frac{C_2\left(d_1-a_{x2}/2\right)}{E_cI_{eff}}]$$

where ε_{edge} is the compressive concrete strain at the middle region of the edge; $\boldsymbol{\alpha}_{ES}$ is the ratio (E_s/E_c).

References

[1] Taylor R, Maher DRH, Hayes B. Effect of the arrangement of reinforcement on the behaviour of reinforced concrete slabs. Magazine of Concrete Research, 1966, 18(55): 85-94.

[2] Ghoneim MG, McGregor JG. Tests of reinforced concrete plates under combined

inplane and lateral loads. ACI Structural Journal, 1994, 91(1): 19-30.

[3] S.J. Foster, C.G. Bailey, I W Burgess, R.J. Plank. Experimental behaviour of concrete floor slabs at large displacements. Engineering Structures, 2004, 26(9): 1231-1247.

[4] Bailey CG, Toh WS. Small-scale concrete slab tests at ambient and elevated temperatures. Engineering Structures, 2007, 29(10): 2775-2791.

[5] K A Cashell, A Y Elghazouli, B A Izzuddin. Failure assessment of lightly reinforced floor slabs. I: experimental investigation. Journal of Structural Engineering, 2011, 137(9): 977-988.

[6] Huang ZH, Burgess IW, Plank RJ. Modeling membrane action of concrete slabs in composite buildings in fire. I: Theoretical development. Journal of Structural Engineering, 2003, 129(8): 1093-1102.

[7] Huang ZH, Burgess IW, Plank RJ. Modeling membrane action of concrete slabs in composite buildings in fire. II: Validations. Journal of Structural Engineering, 2003, 129(8): 1103-1112.

[8] Thomas Gernay, Jean Marc Franssen. A plastic-damage model for concrete in fire: Applications in structural fire engineering. Fire Safety Journal, 2015, 71: 268-278.

[9] Y. Wang, G.L. Yuan, Z.H. Huang, et al., Modelling of reinforced concrete slabs in fire. Fire Safety Journal, 2018, 100: 171-185.

[10] Cameron NJK, Usmani AS. New design method to determine the membrane capacity of laterally restrained composite floor slabs in fire. Part I: Theory and method. The Structural Engineer, 2005, 83(19): 28-33.

[11] Li GQ, Guo SX, Zhou HS. Modeling of membrane action in floor slabs subjected to fire. Engineering Structures, 2007, 29(6): 880-887.

[12] Dong YL, Fang YY. Determination of tensile membrane effects by segment equilibrium. Magazine of Concrete Research, 2010, 62(1): 17-23.

[13] Yong Wang, Wenxuan Guo, Zhaohui Huang, et al. Analytical model for predicting the load-deflection curve of post-fire reinforced-concrete slab. Fire Safety Journal, 2018, 101: 63-83.

[14] Bailey CG, Toh WS. Behavior of concrete floor slabs at ambient and elevated temperatures. Fire Safety Journal, 2010, 42(6-7): 425-436.

[15] Omer E, Izzuddin BA, Elghazouli AY. Failure of unrestrained lightly reinforced concrete slabs under fire - Part I: Analytical models. Engineering Structures, 2010, 32(9): 2631-2646.

[16] K A Cashell, AY Elghazouli, B A Izzuddin. Failure assessment of lightly reinforced floor slabs. II: analytical studies. Journal of Structural Engineering, 2011, 137(9): 989-1001.

[17] Herraiz B, Vogel T. Novel design approach for the analysis of laterally unrestrained reinforced concrete slabs considering membrane action. Engineering Structures, 2016, 123(9): 313-329.

[18] Burgess I. Yield line plasticity and tensile membrane action in lightly-reinforced rectangular concrete slabs. Engineering Structures, 2017, 138(1): 195-214.

[19] Sawczuk A, Winnicki L. Plastic behavior of simply supported reinforced concrete plates at moderately large deflections. International Journal of Solids and Structures,

1965, 1:97-111.

[20] Hayes B. Allowing for membrane action in the plastic analysis of rectangular reinforced concrete slabs. Magazine of Concrete Research, 1968, 20 (65):205-12.

[21] Colin G. Bailey, Wee S. Toh, and Bok M. Chan. Simplified and advanced analysis of membrane action of concrete slabs. ACI Structural Journal, 2008, 105: 30-40.

[22] J. Jiang, G.Q. Li, Parameters affecting tensile membrane action of reinforced-concrete floors subjected to elevated temperatures. Fire Safety Journal, 2018, 96: 59-73.

[23] GB50010-2010: Code for design of concrete structures (2011). China Architecture & Building Press, Beijing, China. (in Chinese).

[24] Ian Burgess, Billy Chan. An integrated yield-line approach to tensile and compressive membrane actions in thin lightly-reinforced concrete slabs. Engineering Structures, 2020, 208, 110321.

[25] O.O.R. Famiyesin, K.M.A. Hossain, Y.H. Chia, P.A. Slade. Numerical and analytical predictions of the limit load of rectangular two way slabs. Computers and Structures, 2001, 79: 43-52.

[26] Matteo Colombo, Paolo Martinelli, Marco di Prisco. A design approach to evaluate the load-carrying capacity of reinforced concrete slabs considering tensile membrane action. Struct Eng Int, 2020, 31(1): 1-11.

[27] Kemp KO. Yield of a square reinforced concrete slab on simple supports, allowing for membrane forces. Struct Eng 1967, 45(7): 235-40.

Captions

Fig. 1 Schematic diagram of membrane action and plate division.

Fig. 2 Failure modes, plates and internal forces distribution in the concrete slab (a) Plate ①; (b) Plate ②; and (c) Plate ③.

Fig. 3 Internal forces on the cross section along the thickness of the concrete slab (a) Plate ① and (b) Plate ②.

Fig. 4 Internal forces on the plates of the concrete slab (a) Plate ① and (b) Plate ②.

Fig. 5 Two distances proposed in the model. (a) Horizontal distance x' (from Point B); (b) Vertical distance y' (from Point A).

Fig. 6 Flow chart for calculating the ultimate loads of the concrete slab.

Fig. 7 Comparison of measured and analytical results of concrete slabs predicted by different methods.

Fig. 8 Two failure modes of the concrete slab [4-5, 19-20].

Fig. 9 Comparison of tensile membrane action region predicted by the present and numerical methods (membrane traction: red = tension, blue = compression; red circles: predicted by present method).

Fig. 10 Cracks on the bottom surface of two slabs [20].

Table 1 Material properties of reinforced concrete slabs.

Table 2 Measured and calculated ultimate loads of concrete slabs.

Table 3 Membrane action region of the slabs based on the proposed methods and Vulcan.

Table 4 Concrete strains and failure mode of the slabs predicted by the present and

Bailey method.

Fig. 1

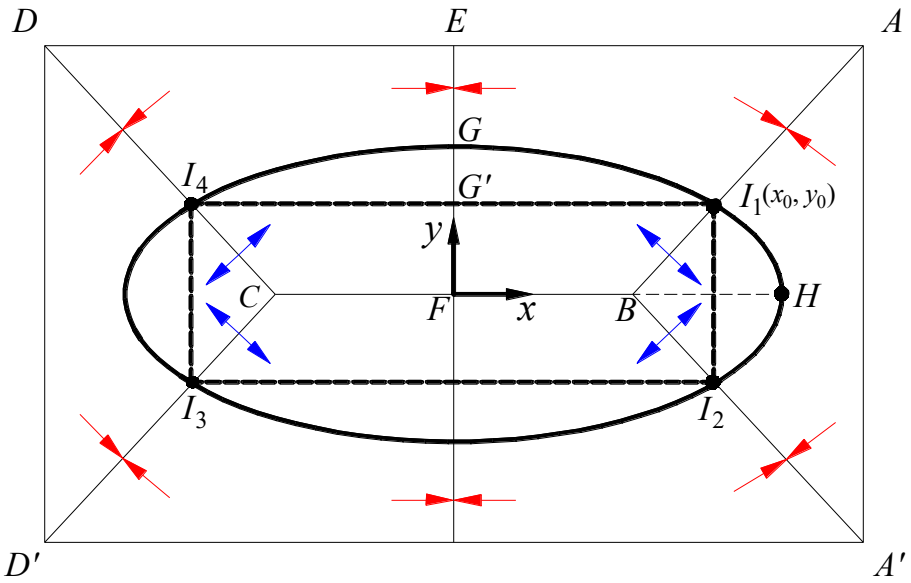

(a) The central ellipse region of tensile membrane tractions in the slab at ultimate limited state

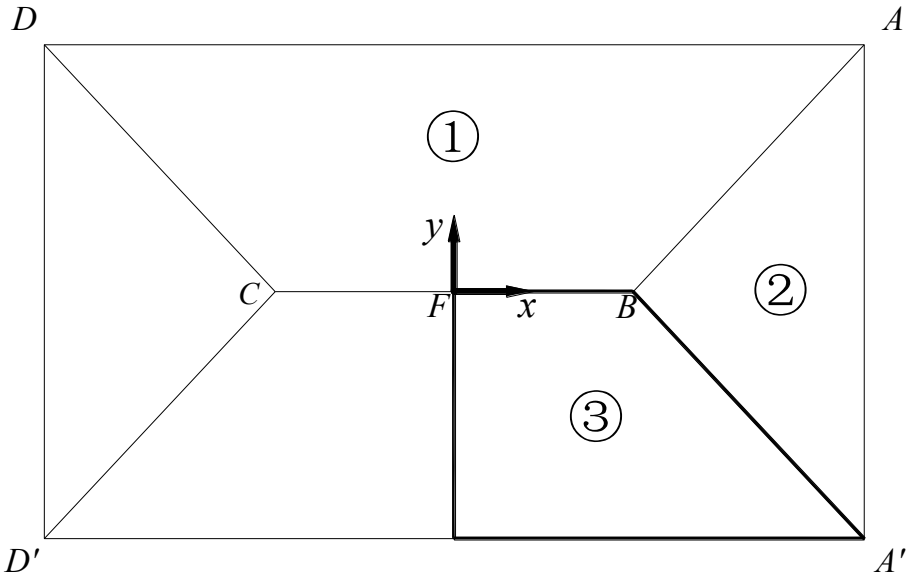

(b) Plate division diagram

Fig. 1 Schematic diagram of membrane action and plate division

Fig. 2

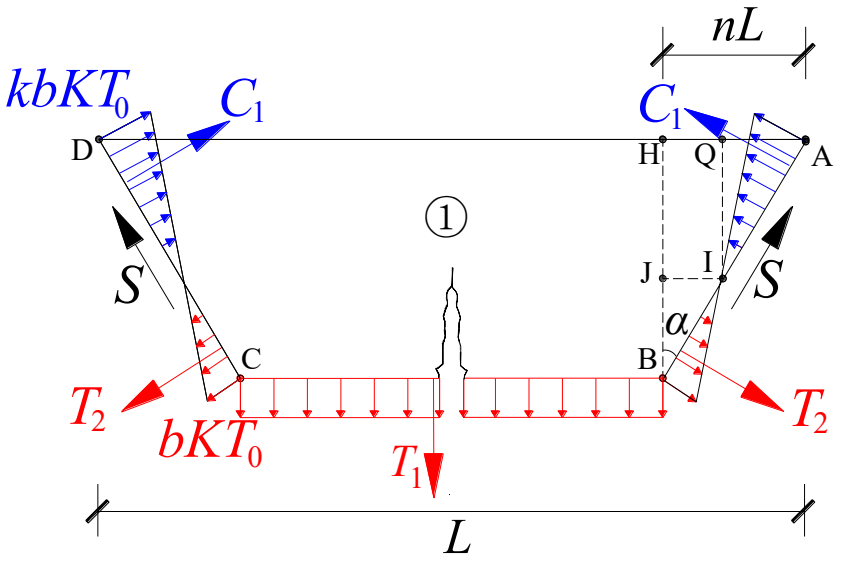

(a) Plate ①

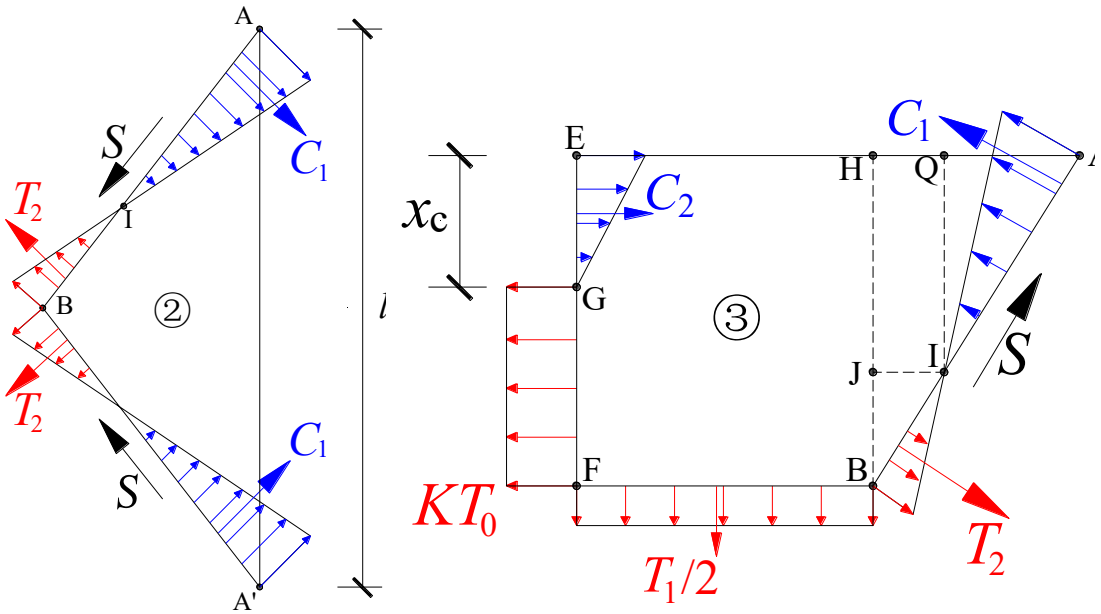

(b) Plate ②

(c) Plate ③

Fig. 2 Failure modes, plates and internal forces distribution in the concrete slab

Fig. 3

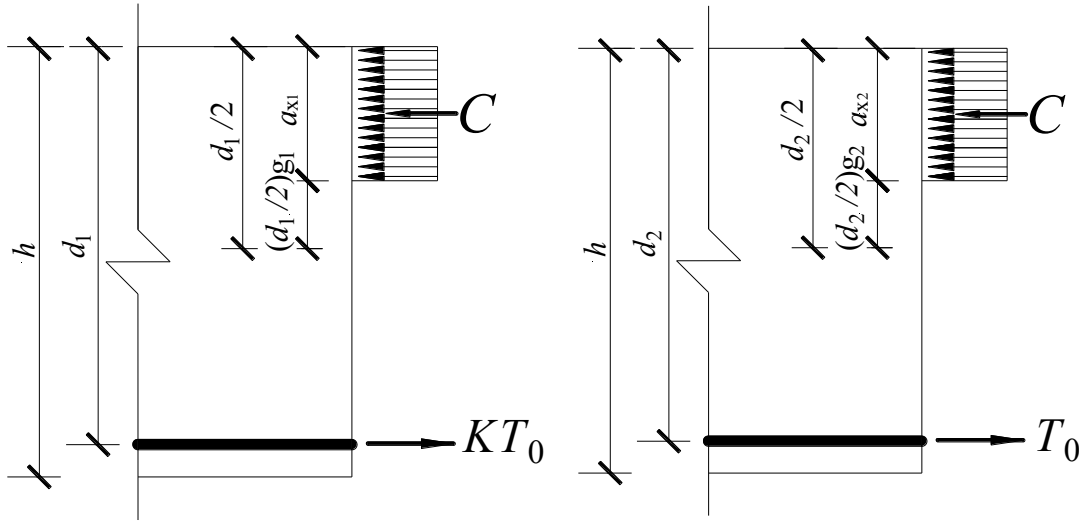

(a) Plate ① (b) Plate ②

Fig. 3 Internal forces on the cross section along the thickness of the concrete slab

Fig. 4

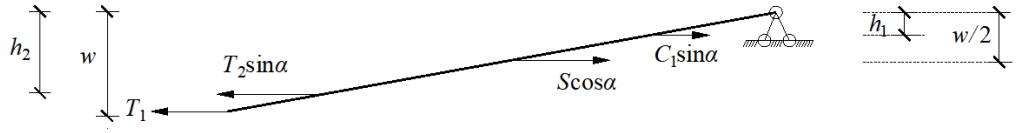

$$h_1 = \frac{\frac{1}{3}\times\frac{k}{1+k}\times\sqrt{(nL)^2+(l/2)^2}\times\frac{l/2}{\sqrt{(nL)^2+(l/2)^2}}}{l/2}\times w$$

$$h_2 = \frac{\frac{l}{2}-\frac{1}{3}\times\frac{1}{1+k}\times\sqrt{(nL)^2+\frac{l^2}{4}}\times\frac{\frac{l}{2}}{\sqrt{(nL)^2+\frac{l^2}{4}}}}{\frac{l}{2}}\times w$$

(a) Plate ①

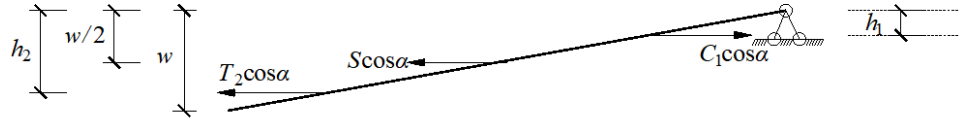

$$h_1 = \frac{\frac{1}{3}\times\frac{k}{1+k}\times\sqrt{(nL)^2+(l/2)^2}\times\frac{nL}{\sqrt{(nL)^2+(l/2)^2}}}{nL}\times w$$

$$h_2 = \frac{nL-\frac{1}{3}\times\frac{1}{1+k}\times\sqrt{(nL)^2+(l/2)^2}\times\frac{nL}{\sqrt{(nL)^2+(l/2)^2}}}{nL}\times w$$

(b) Plate ②

Fig. 4 Internal forces on the plates of the concrete slab

Fig. 5

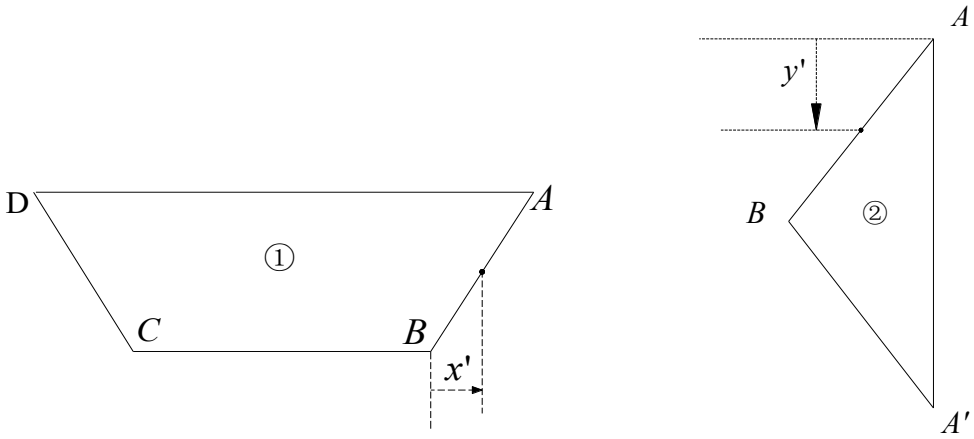

(a) Horizontal distance x' (from Point B) (b) Vertical distance y' (from Point A)

Fig. 5 Two distances proposed in the model

Fig. 6

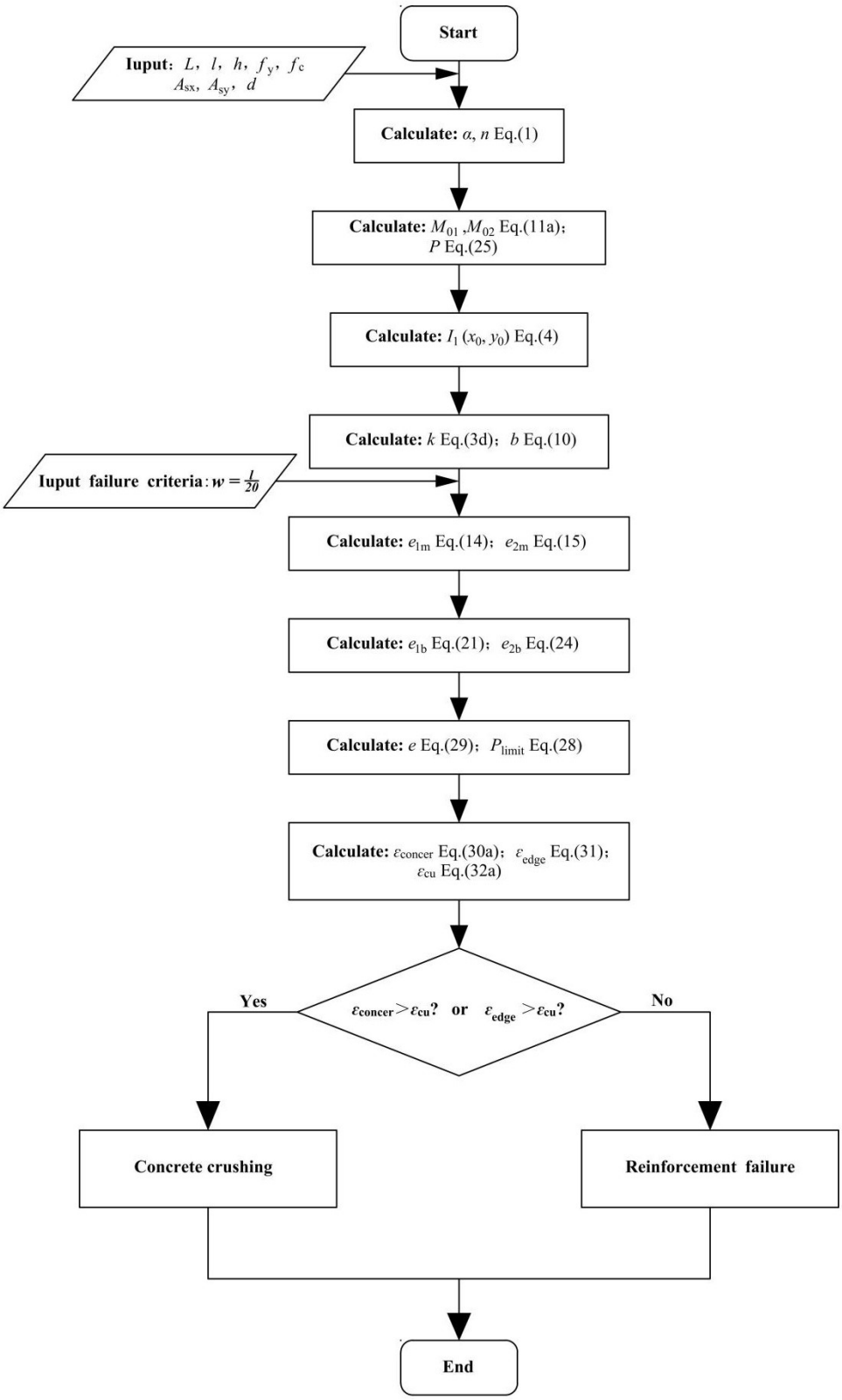

Fig. 6 Flow chart for calculating the ultimate loads of the concrete slab

Fig. 7

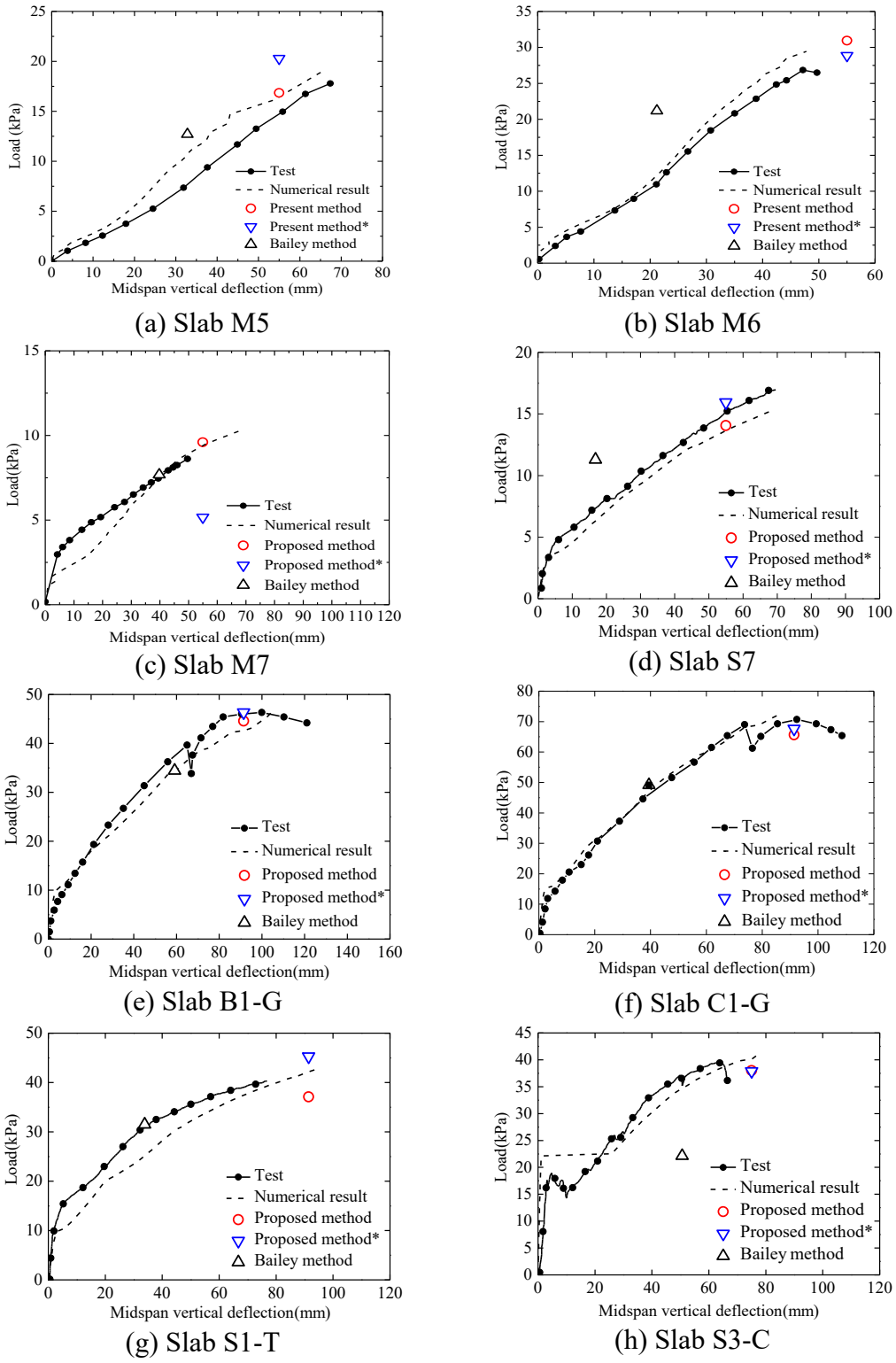

Fig. 7 Comparison of measured and analytical results of concrete slabs predicted by different methods

Fig. 8

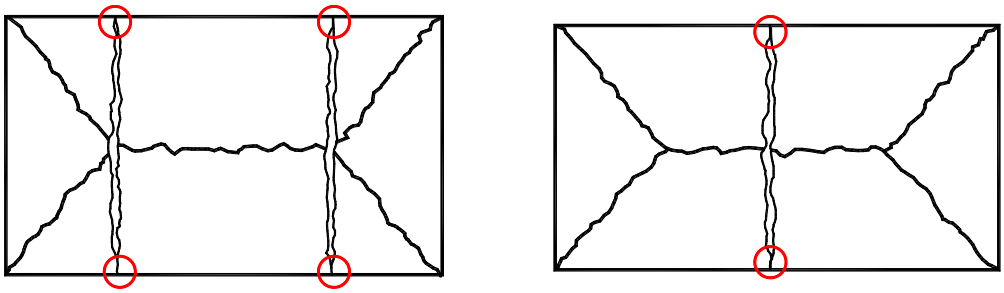

(a) Mode 1 (b) Mode 2

Fig. 8 Two failure modes of the concrete slab [4-5, 19-20]

Fig. 9

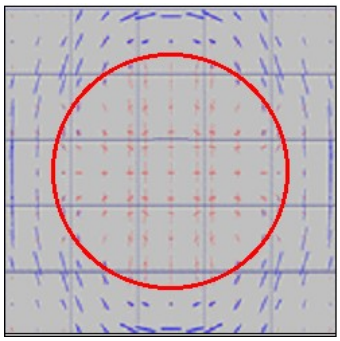

(a) Slab S1-T (at 42.14 kPa)

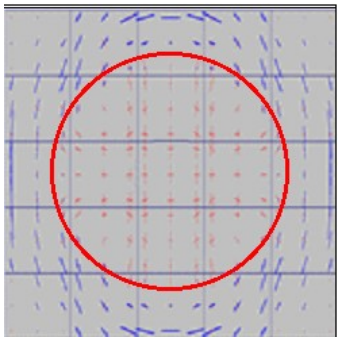

(b) Slab S6-T (at 39.20 kPa)

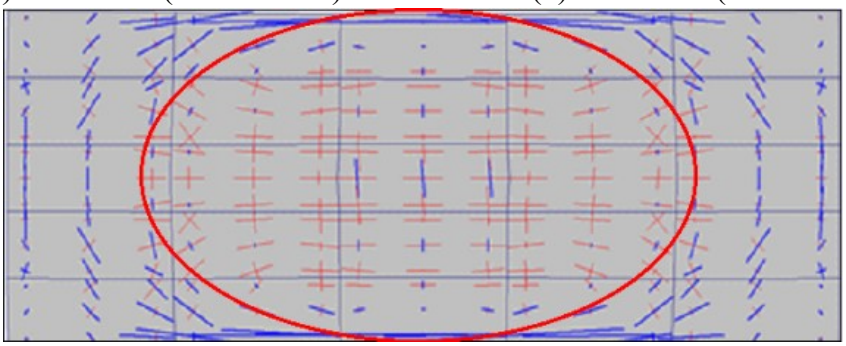

(c) Slab A1-G (at 29.08 kPa)

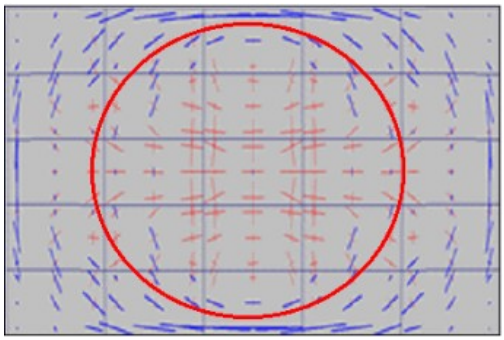

(d) Slab B1-G (at 42.69 kPa)

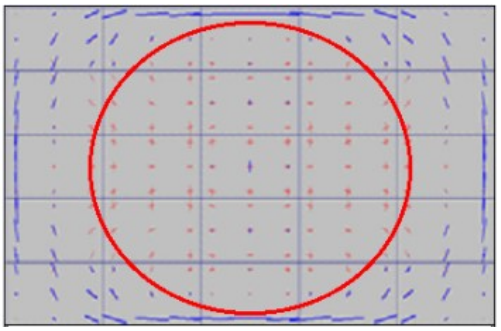

(e) Slab M1 (at 16.97 kPa)

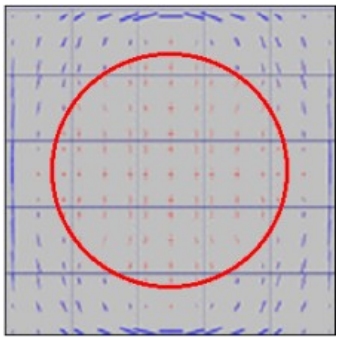

(f) Slab M2 (at 28.54 kPa)

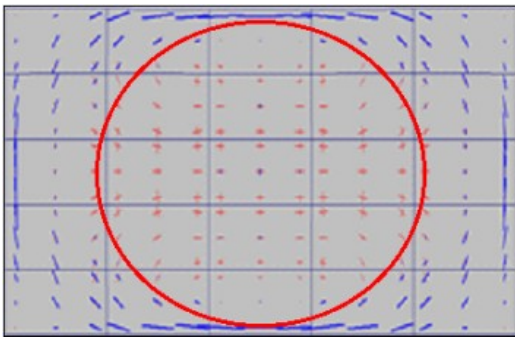

(g) Slab S1 (at 24.25 kPa)

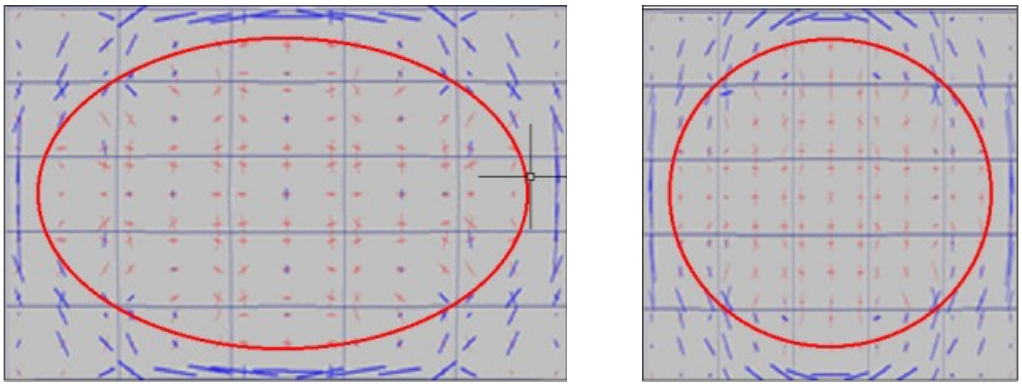

(h) Slab R1-C (at 25.80 kPa) (i) Slab S3-C (at 40.10 kPa)

Fig. 9 Comparison of tensile membrane action region predicted by the present and numerical methods (membrane traction: red = tension, blue = compression; red circles: predicted by present method)

Fig. 10

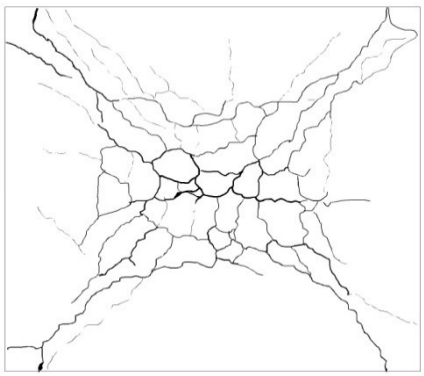

(a) Square slab

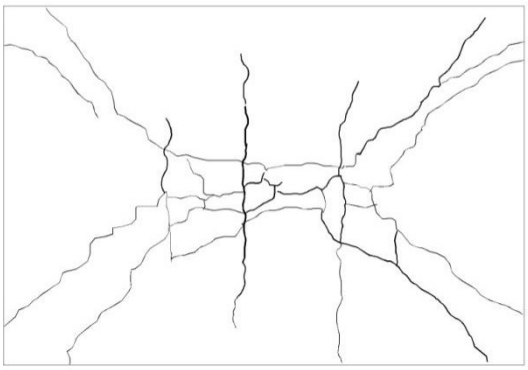

(b) Rectangular slab

Fig. 10 Cracks on the bottom surface of two slabs [20]

Tables

Table 1 Material properties of reinforced concrete slabs

Reference	Slab	$L\times l\times h$ (mm)	Material properties						f_{cu} (MPa)	d_1 (mm)	d_2 (mm)
			E_s(GPa)	$f_{y,x}$(MPa)	$f_{y,y}$ (MPa)	A_{sx}(mm^2/m)	A_{sy} (mm^2/m)	Diameter (mm)			
Taylor [1]	S1-T	1829×1829×50.8	206.0	375.9	375.9	233.50	280.20	4.76	35.0	43.66	38.90
	S6-T	1829×1829×50.8	206.0	420.8	420.8	200.00	233.50	4.76	35.6	43.66	38.90
	S7-T	1829×1829×44.5	206.0	375.9	375.9	280.20	320.00	4.76	38.2	37.36	32.60
	S9-T	1829×1829×76.2	206.0	375.9	375.9	142.00	160.00	4.76	33.2	69.06	64.30
Ghoneim [2]	A1-G	4627×1829×67.3	181.5	450.0	450.0	260.00	260.00	6.35	27.8	54.50	48.15
	B1-G	2745×1829×68.2	181.5	450.0	450.0	260.00	260.00	6.35	23.4	55.00	48.65
	C1-G	1829×1829×67.8	181.5	450.0	450.0	260.00	260.00	6.35	31.5	56.80	50.45
	D1-G	1829×1829×92.8	181.5	450.0	450.0	364.00	364.00	6.35	32.6	82.70	76.35
Bailey [4]	M1	1700×1100×18.2	205.0	732.0	757.0	90.50	90.50	2.42	41.3	12.00	9.57
	M2	1100×1100×19.1	205.0	732.0	757.0	90.50	90.50	2.42	38.0	12.90	10.40
	M3	1700×1100×22.0	205.0	451.0	454.0	68.60	72.40	1.53	35.3	16.20	14.70
	M4	1100×1100×20.1	205.0	451.0	454.0	68.60	72.40	1.53	35.3	14.30	12.80
	M5	1700×1100×18.9	205.0	406.0	435.0	135.50	133.60	1.47	37.9	13.20	11.70
	M6	1100×1100×21.6	205.0	406.0	435.0	135.50	133.60	1.47	38.6	15.90	14.40
	M7	1700×1100×20.4	205.0	599.0	604.0	44.70	43.60	0.84	41.6	15.00	14.10
	M8	1100×1100×19.0	205.0	599.0	604.0	44.70	43.60	0.84	42.9	13.60	12.70
	M9	1700×1100×22.0	205.0	450.0	402.0	57.20	53.90	0.66	37.6	16.70	16.00
	M10	1100×1100×19.4	205.0	450.0	402.0	57.20	53.90	0.66	37.3	14.10	13.40
	S1	1700×1100×19.0	205.0	639.0	614.0	139.10	138.20	2.99	40.6	12.50	9.51
	S2	1100×1100×20.4	205.0	639.0	614.0	139.10	138.20	2.99	41.2	13.90	10.90
	S3	1700×1100×21.0	205.0	569.0	555.0	97.40	97.40	2.51	50.0	14.70	12.20
	S4	1100×1100×19.0	205.0	569.0	555.0	97.40	97.40	2.51	50.7	12.70	10.20
	S5	1700×1100×17.6	205.0	344.0	447.0	72.40	74.30	1.55	49.8	11.80	10.30
	S6	1100×1100×20.6	205.0	344.0	447.0	74.30	72.40	1.53	49.8	14.80	13.30
	S7	1700×1100×20.5	205.0	265.0	271.0	154.40	154.40	1.58	41.9	14.70	13.10
	S8	1100×1100×19.3	205.0	265.0	271.0	154.40	154.40	1.58	43.0	13.50	11.90
	S9	1700×1100×19.7	205.0	280.0	301.0	94.30	94.30	0.98	37.1	14.20	13.20
	S10	1100×1100×18.8	205.0	280.0	301.0	94.30	94.30	0.98	37.2	13.30	12.30
Cashell [5]	R1-C	2250×1500×60	205.0	552.0	552.0	141.40	141.37	6.00	44.4	30.00	24.00
	S3-C	1500×1500×60	205.0	552.0	552.0	141.37	141.37	6.00	44.4	30.00	24.00

R6-C	2250×1500×60	205.0	553.0	553.0	141.37	282.74	6.00	32.0	30.00	24.00
S7-C	1500×1500×60	205.0	553.0	553.0	141.37	141.37	6.00	33.0	30.00	24.00

Table 2 Measured and calculated ultimate loads of concrete slabs

* The in-plane shear force is not considered.

Reference	Slab	P_{test}/kPa	δ_{test} /mm	δ_{limit} /mm			P_{limit} /kPa					P_{limit}/P_{test}				
				Bailey method	Present method	Yield line	Bailey	Vulcan	Present *	Present	Yield line	Bailey	Vulcan	Present *	Present
Taylor [1]	S1-T	42.90	81.3	33.8	91.45	26.76	32.61	42.14	45.39	44.70	0.62	0.76	0.98	0.94	1.04
	S6-T	39.60	81.3	35.7	91.45	25.40	31.29	39.20	42.61	42.13	0.64	0.79	0.99	0.92	1.06
	S7-T	39.00	97.9	33.8	91.45	26.00	33.23	43.85	45.83	46.09	0.67	0.85	1.12	0.97	1.18
	S9-T	38.10	83.8	33.8	91.45	26.49	30.00	34.30	40.25	38.51	0.70	0.79	0.90	1.04	1.01
Ghoneim [2]	A1-G	39.69	132.4	99.8	91.45	23.62	24.94	29.08	34.47	36.27	0.60	0.63	0.73	0.87	0.91
	B1-G	45.90	101.2	59.2	91.45	27.54	35.93	42.69	46.10	44.40	0.60	0.78	0.93	0.95	0.97
	C1-G	73.90	91.2	39.4	91.45	41.87	51.52	75.36	68.08	66.15	0.57	0.70	1.02	0.94	0.90
	D1-G	109.40	101.7	39.4	91.45	87.53	100.85	123.10	132.96	127.14	0.80	0.92	1.13	0.98	1.16
Bailey [4]	M1	20.74	72.5	44	55	8.52	15.50	16.97	20.68	18.88	0.41	0.75	0.82	1.00	0.91
	M2	26.99	60.4	28.5	55	13.80	20.30	28.54	29.88	31.72	0.51	0.75	1.06	1.11	1.18
	M3	12.28	85.4	34.5	55	6.35	9.13	9.72	12.88	11.80	0.52	0.74	0.79	1.05	0.96
	M4	18.29	65.2	22.3	55	8.17	11.90	17.75	15.78	16.66	0.45	0.65	0.97	0.86	0.91
	M5	17.92	68.1	32.8	55	8.69	12.70	16.29	20.26	17.90	0.48	0.71	0.91	1.13	1.00
	M6	27.03	48	21.2	55	15.72	21.20	28.62	28.88	30.97	0.58	0.78	1.06	1.07	1.15
	M7	8.65	49.7	39.8	55	5.11	7.68	8.09	10.88	9.61	0.59	0.89	0.94	1.26	1.11
	M8	10.70	29.8	25.8	55	6.68	10.10	13.54	12.62	13.62	0.62	0.94	1.27	1.18	1.27
	M9	7.35	22	34.5	55	5.07	7.16	9.89	10.13	9.20	0.69	0.97	1.35	1.38	1.25
	M10	9.89	19.6	22.3	55	6.36	9.13	12.54	11.64	12.40	0.64	0.92	1.27	1.18	1.25
	S1	17.14	61	41.1	55	10.62	16.50	24.25	25.24	23.82	0.62	0.96	1.41	1.48	1.39
	S2	26.81	46.5	26.6	55	18.66	25.50	32.00	41.00	42.39	0.70	0.95	1.19	1.53	1.58
	S3	17.31	89.5	38.8	55	9.20	15.70	17.16	19.59	18.07	0.53	0.91	0.99	1.13	1.04
	S4	22.78	70.9	25.1	55	11.59	20.70	31.00	25.07	26.17	0.51	0.91	1.36	1.10	1.15
	S5	13.35	186.5	30.2	55	4.23	7.20	9.01	10.77	8.86	0.32	0.54	0.67	0.80	0.66
	S6	26.78	138.2	22.2	55	7.76	12.70	19.35	14.92	15.78	0.29	0.47	0.72	0.56	0.59
	S7	19.48	176.6	26.5	55	7.37	11.30	13.80	15.87	14.25	0.38	0.58	0.71	0.81	0.73
	S8	35.98	166.5	17.1	55	9.84	15.70	23.75	19.36	20.72	0.27	0.44	0.66	0.54	0.58
	S9	14.26	168.9	27.2	55	4.94	7.84	8.98	10.13	9.52	0.35	0.55	0.63	0.76	0.67
	S10	20.18	62.7	17.6	55	6.66	10.80	15.50	12.72	13.82	0.33	0.54	0.77	0.63	0.68
Cashell [5]	R1-C	25.61	—	50.6	75	16.54	21.13	25.80	26.29	27.79	0.65	0.83	1.01	1.03	1.08
	S3-C	40.76	64	33.7	75	24.10	29.52	40.10	35.37	38.31	0.59	0.72	0.98	0.87	0.94
	R6-C	29.31	—	50.6	75	16.34	23.14	25.60	32.01	31.47	0.56	0.79	0.87	1.09	1.07
	S7-C	40.72	84	33.7	75	23.85	29.10	40.80	35.03	38.02	0.59	0.71	1.00	0.86	0.93
Average	-	-	-	-	-	-	-	-	-	-	0.54	0.76	0.96	0.92	0.98
COV	-	-	-	-	-	-	-	-	-	-	0.25	0.20	0.22	0.29	0.21

Table 3 Membrane action region of the slabs based on the proposed methods and Vulcan

Reference	Slab	Present method			Vulcan			A_P/A_F-
		x_0 (m)	y_0 (m)	A_P (m^2)	x_0 (m)	y_0 (m)	A_F (m^2)	
Taylor [1]	S1-T	0.453	0.461	1.314	0.483	0.476	1.446	0.91
	S6-T	0.464	0.451	1.315	0.473	0.459	1.365	0.96
	S7-T	0.458	0.457	1.314	0.462	0.461	1.340	0.98
	S9-T	0.458	0.457	1.314	0.438	0.437	1.204	1.09
Ghoneim [2]	A1-G	1.491	0.288	5.231	1.519	0.309	3.543	1.48
	B1-G	0.772	0.388	2.245	0.815	0.425	2.188	1.03
	C1-G	0.465	0.450	1.315	0.499	0.485	1.521	0.86
	D1-G	0.462	0.453	1.314	0.468	0.458	1.360	0.97
Bailey [4]	M1	0.457	0.244	0.826	0.534	0.260	0.896	0.92
	M2	0.282	0.268	0.477	0.308	0.290	0.567	0.84
	M3	0.461	0.241	0.830	0.503	0.245	0.824	1.01
	M4	0.281	0.270	0.476	0.308	0.297	0.576	0.83
	M5	0.468	0.237	0.836	0.508	0.248	0.857	0.98
	M6	0.276	0.274	0.475	0.310	0.300	0.587	0.81
	M7	0.470	0.236	0.838	0.467	0.227	0.701	1.20
	M8	0.276	0.274	0.475	0.301	0.297	0.564	0.84
	M9	0.465	0.239	0.833	0.495	0.266	0.856	0.97
	M10	0.279	0.272	0.476	0.297	0.290	0.540	0.88
	S1	0.449	0.250	0.819	0.502	0.229	0.759	1.08
	S2	0.286	0.265	0.478	0.289	0.271	0.492	0.97
	S3	0.457	0.244	0.825	0.529	0.266	0.936	0.88
	S4	0.285	0.266	0.478	0.328	0.315	0.652	0.73
	S5	0.478	0.232	0.846	0.519	0.232	0.841	1.01
	S6	0.279	0.271	0.476	0.288	0.264	0.479	0.99
	S7	0.465	0.239	0.833	0.520	0.262	0.862	0.97
	S8	0.279	0.271	0.476	0.267	0.255	0.429	1.11
	S9	0.471	0.235	0.840	0.529	0.270	0.899	0.93
	S10	0.275	0.275	0.475	0.316	0.307	0.612	0.78
Cashell [5]	R1-C	0.643	0.313	1.524	0.748	0.408	1.934	0.79
	S3-C	0.387	0.365	0.887	0.454	0.436	1.245	0.71
	R6-C	0.644	0.313	1.524	0.764	0.373	1.871	0.81
	S7-C	0.387	0.364	0.887	0.453	0.435	1.239	0.72

Table 4 Concrete strains and failure mode of the slabs predicted by the present and Bailey method

Reference	Slab	ε_{cu} (10^{-3})	Present *(10^{-3})		Present (10^{-3})		Failure mode			
			ε_1	ε_2	ε_1	ε_2	Bailey	Present *	Present	Test
Taylor [1]	S1-T	3.841	3.257	2.235	3.401	1.564	—	R	C	—
	S6-T	3.834	3.268	2.246	3.403	1.572	—	R	C	—
	S7-T	3.759	3.479	2.378	3.644	1.664	—	C	C	—
	S9-T	3.899	3.058	2.158	3.093	1.510	—	R	R	—
Ghoneim [2]	A1-G	4.179	2.967	1.918	2.715	1.343	—	R	R	—
	B1-G	4.627	2.632	1.723	2.538	1.206	—	R	R	—
	C1-G	3.970	3.052	2.081	3.138	1.457	—	R	R	—
	D1-G	3.923	3.091	2.130	3.164	1.491	—	R	R	—
Bailey [4]	M1	3.704	4.254	2.521	3.968	1.758	C	C	C	R
	M2	3.765	3.970	2.367	4.408	1.657	C	C	C	C
	M3	3.832	3.278	2.248	3.215	1.574	R	R	R	R
	M4	3.832	3.274	2.248	3.336	1.574	R	R	R	C
	M5	3.767	3.688	2.362	3.516	1.654	R	C	C	C
	M6	3.752	3.532	2.393	3.733	1.675	R	C	C	C
	M7	3.699	3.700	2.525	3.616	1.768	R	C	C	R
	M8	3.681	3.729	2.582	3.823	1.808	R	C	C	R
	M9	3.773	3.374	2.349	3.326	1.644	R	R	R	C
	M10	3.780	3.348	2.336	3.377	1.635	R	R	R	R
	S1	3.715	4.185	2.481	3.898	1.737	C	C	C	C
	S2	3.705	4.185	2.508	4.374	1.755	C	C	C	C
	S3	3.615	4.294	2.895	4.187	2.026	R	C	C	C
	S4	3.611	4.384	2.926	4.486	2.048	R	C	C	C
	S5	3.616	4.237	2.886	4.170	2.020	R	C	C	C
	S6	3.616	4.126	2.886	4.271	2.020	R	C	C	C
	S7	3.695	3.669	2.538	3.615	1.777	R	C	C	C
	S8	3.679	3.713	2.587	3.780	1.811	R	C	C	C
	S9	3.785	3.365	2.327	3.314	1.629	R	R	R	C
	S10	3.783	3.333	2.332	3.408	1.632	R	R	C	C
Cashell [5]	R1-C	3.662	4.045	2.648	3.824	1.854	—	C	C	—
	S3-C	3.662	3.889	2.648	3.971	1.854	—	C	C	—
	R6-C	3.948	3.927	2.103	4.804	1.472	—	C	C	—
	S7-C	3.908	3.257	2.147	3.373	1.503	—	R	R	—

* The in-plane shear force is not considered.